Acta Pharmaceutica Sinica B 2021;11(7):2004–2015

Chinese Pharmaceutical Association
Institute of Materia Medica, Chinese Academy of Medical Sciences

Acta Pharmaceutica Sinica B

www.elsevier.com/locate/apsb
www.sciencedirect.com

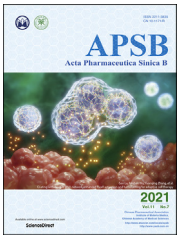

ORIGINAL ARTICLE

Synergetic delivery of triptolide and Ce6 with light-activatable liposomes for efficient hepatocellular carcinoma therapy

Ling Yu[a,†], Zhenjie Wang[b,†], Zhuomao Mo[a], Binhua Zou[c], Yuanyuan Yang[c], Rui Sun[c], Wen Ma[c], Meng Yu[c,*], Shijun Zhang[a,*], Zhiqiang Yu[c,*]

[a]*Department of Traditional Chinese Medicine, the First Affiliated Hospital, Sun Yat-sen University, Guangzhou 510080, China*
[b]*The People's Hospital of Gaozhou, Maoming 525200, China*
[c]*School of Pharmaceutical Sciences, Guangdong Provincial Key Laboratory of New Drug Screening, Southern Medical University, Guangzhou 510515, China*

Received 27 October 2020; received in revised form 11 December 2020; accepted 10 January 2021

KEY WORDS

Hepatocellular carcinoma;
Synergetic delivery;
Triptolide;
Ce6;
Photo-activatable liposomes;

Abstract Hepatocellular carcinoma (HCC) has been known as the second common leading cancer worldwide, as it responds poorly to both chemotherapy and medication. Triptolide (TP), a diterpenoid triepoxide, is a promising treatment agent for its effective anticancer effect on multiple cancers including HCC. However, its clinical application has been limited owing to its severe systemic toxicities, low solubility, and fast elimination in the body. Therefore, to overcome the above obstacles, photo-activatable liposomes (LP) integrated with both photosensitizer Ce6 and chemotherapeutic drug TP (TP/Ce6-LP) was designed in the pursuit of controlled drug release and synergetic photodynamic therapy in HCC

Abbreviations: ALT, liver-related alanine aminotransferase; AST, aspartate aminotransferase; BCA, bicinchoninic acid; BUN, blood urea nitrogen; Chol, cholesterol; CK, creatine kinase; CK-MB, creatine kinase-MB; CLSM, confocal laser scanning microscopy; Cr, creatinine; DEE, drug encapsulation efficiency; DLC, drug loading content; DLS, dynamic light scattering; Dox, doxorubicin; DSPG, distearoyl phosphatidylglycerole; EPR, enhanced permeability and retention; FBS, fetal bovine serum; FCM, flow cytometry; HCC, hepatocellular carcinoma; LDH, lactate dehydrogenase; LP, liposomes; NIR, near-infrared; PDT, photodynamic therapy; PDX, patient-derived xenograft; PDXHCC, patient derived tumor xenograft of HCC; PI, propidium iodide; Pt, platinum; ROS, reactive oxygen species; So, sorafenib; TEM, transmission electron microscope; TP, triptolide; TP/Ce6-LP, liposomes integrated with both photosensitizer Ce6 and chemotherapeutic drug TP; TUNEL, dT-mediated dUTP Nick-End Labeling.

*Corresponding authors.
E-mail addresses: yumeng999@smu.edu.cn (Meng Yu), zhshjun@mail.sysu.edu.cn (Shijun Zhang), yuzq@smu.edu.cn (Zhiqiang Yu).
[†]These authors made equal contributions to this work.

Peer review under responsibility of Chinese Pharmaceutical Association and Institute of Materia Medica, Chinese Academy of Medical Sciences.

https://doi.org/10.1016/j.apsb.2021.02.001

Photosensitizer;
Process of photodynamic therapy;
PDX model

therapy. The TP encapsulated in liposomes accumulated to the tumor site due to the enhanced permeability and retention (EPR) effect. Under laser irradiation, the photosensitizer Ce6 generated reactive oxygen species (ROS) and further oxidized the unsaturated phospholipids. In this way, the liposomes were destroyed to release TP. TP/Ce6-LP with NIR laser irradiation (TP/Ce6-LP+L) showed the best anti-tumor effect both *in vitro* and *in vivo* on a patient derived tumor xenograft of HCC (PDXHCC). TP/Ce6-LP significantly reduced the side effects of TP. Furthermore, TP/Ce6-LP+L induced apoptosis through a caspase-3/PARP signaling pathway. Overall, TP/Ce6-LP+L is a novel potential treatment option in halting HCC progression with attenuated toxicity.

1. Introduction

Hepatocellular carcinoma (HCC) occurs after long-term liver disease, and has become the most prevalent form of primary liver cancer[1]. HCC constitutes the second largest cause of cancer mortality in many countries[2]. Thus, it is one of massive global health problems today[3]. Up to now, in order to cure HCC, many strategies have been extensively employed, such as hepatic resection, orthotopic liver transplantation, chemoembolization, transarterial embolization and biotherapies[4,5]. However, the survival rate of HCC patient remains poor till far, due to the limitations of present strategies[6]. For example, less than 30% of patients are reported to receive specific interventions after liver transplantation, surgery, or chemoembolization[7]. Moreover, systemic chemotherapies lack target selectivity and are typically accompanied with multi-drug resistance as well as other severe side effects[8−10]. Therefore, the dismal prognosis for most HCC patients emphasizes a pressing need for new and efficient therapeutic strategies against HCC. Recently, traditional Chinese medicine has received increasing attention due to its broad-spectrum anti-inflammatory and anti-cancer activities. In particular, triptolide (TP), a biological diterpenoid triepenoid isolated from the plant *Tripterygium wilfordii*, is a promising chemotherapeutic agent[11]. Studies suggest that low concentrations of TP can effectively inhibit the growth of malignant cancers including HCC[12−15]. Nonetheless, its clinical application has been limited by its severe systemic toxicities, low solubility, narrow therapeutic window, and unclear therapeutic targets[16,17]. Therefore, there is an urgent need to develop a TP delivery system for treatment of HCC with high efficiency and low toxicity.

Over the past decade, stimuli-responsive nanomedicine has experienced intensive development in pursuit of better therapeutic potency and attenuated toxicity[18−22]. The advantages of stimuli-responsive nanomedicine include excellent stability, improved tumor accumulation, desirable endocytosis, as well as preferable drug release capacity[18,23−25]. Particularly, these systems are capable of releasing therapeutic cargos responsive to not only endogenous stimuli (*e.g.*, pH and ROS, etc. in the microenvironment of tumors), but also external stimuli (temperature, electromagnetic radiation and acoustic ultrasound, etc.)[18,26]. Light-responsive liposomes are especially attractive due to their controllability, availability and low toxicity[27,28]. For example, while photosensitizes were almost non-toxic to the human body, they generated ROS within the liposomes under light irradiation[29,30]. ROS plays a direct role in the process of photodynamic therapy (PDT)[31,32], where it causes peroxidation of unsaturated phospholipids and, thus, renders them hydrophilic, resulting in the release of encapsulated drugs[26,33]. Ce6, a near-infrared (NIR) photosensitizer, can produce ROS under 650 nm laser irradiation for PDT. Therefore, the combined application of Ce6 and TP will benefit from the reduced toxicity *via* light controlled rapid release of TP specifically at the tumor site. Moreover, a patient-derived tumor xenograft (PDX) model of HCC (PDXHCC) was used to explore the potential of TP/Ce6-LP under light irradiation for effective anti-tumor therapy. The PDX model had the following advantages that could not only maintain biological stability and intratumoral heterogeneity, but also regenerated a microenvironment similar to the human tumor (for example, tumor vasculature, extracellular matrix and macrophages)[34,35]. Therefore, the PDX model could more accurately evaluate the therapeutic effect of nanomedicine.

Herein, we designed photo-activatable liposomes incorporating Ce6 and TP (TP/Ce6-LP) for HCC therapy (Scheme 1). First, the structure of the allylic hydrogens in egg yolk lecithin (PC-98T) could react with ROS generated by Ce6 to form reversible lipid peroxides upon near-infrared (NIR) laser irradiation, making the liposomal components hydrophilic to release TP. Afterwards, the oxygen-dependent PDT and TP-based chemotherapeutics exerted potent anti-tumor effect on the PDXHCC model. In addition, free TP caused severe liver damage, while TP/Ce6-LP reduced the hepatotoxicity of it. Therefore, our proposed TP/Ce6-LP was envisioned to not only enhance therapeutic efficiency but also reduce toxic effects of TP. Finally, TP/Ce6-LP under light irradiation possibly induced cell apoptosis *via* a caspase-3/PARP signaling pathway.

2. Materials and methods

2.1. Material

Triptolide was purchased from Chengdu Biopurify Phytochemicals Ltd. Cholesterol (Chol), distearoyl phosphatidylglycerole (DSPG) and egg yolk lecithin (PC-98T) were sourced from AVT (Shanghai) Pharmaceutical Tech Co., Ltd., Shanghai, China. GSH and GSSG assay kit, Annexin V-FITC/Propidium iodide (PI) Apoptosis Detection Kit, Cell Cycle and Apoptosis Analysis Kit, Bicinchoninic Acid (BCA) Protein Assay Kit and goat anti-rabbit IgG/HRP antibody were obtained from Beyotime Institute of Biotechnology, Nanjing, China. Reactive Oxygen Species Assay Kit was purchased from Beijing Solarbio Science & Technology Co., Ltd., Beijing, China. RPMI 1640 medium, trypsin, and fetal bovine serum (FBS) were provided by Gibco BRL, USA. Anti-caspase-3 antibody and anti-PARP-1 antibody were soured from Cell Signaling Technology, USA. Anti-GAPDH (glyceraldehyde-

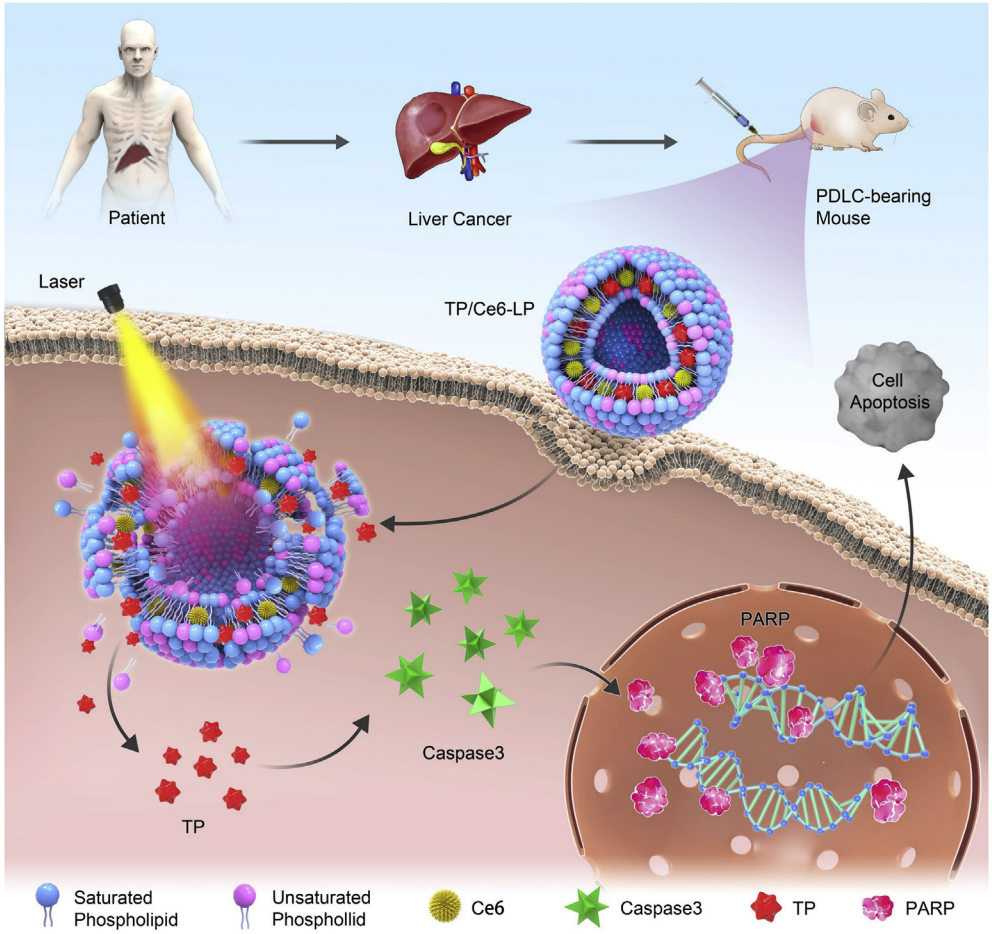

Scheme 1 Schematic illustration of preparation, targeting mechanism, synchronous intracellular drug release, and visualization of photosensitive liposome@TP (TP/Ce6-LP).

3-phosphate dehydrogenase) rabbit monoclonal antibody was purchased from WuXi AppTec, Shanghai, China.

2.2. *Preparation of liposome*

The ratio of Chol:DSPG:PC-98T was 1:1:1 in the blank liposomes. LPs loaded with TP and Ce6 (TP/Ce6-LPs) were prepared as the following: first, 30 mg of lipid materials, 4 mg TP, and 0.06 mg Ce6 were dissolved in 12 mL of a mixed organic solvent (chloroform:methanol = 5:1, *v*/*v*); then, the solvent was removed using a spin evaporator under reduced pressure at 60 °C; next, the dry mixture was hydrated with 5 mL water under sonication and then the mixture was extruded at room temperature; finally, the obtained TP/Ce6-LPs were dialyzed (MWCO = 3500 Da) for 6 h to remove the free drug.

2.3. *Characterization*

The morphology and size of LPs were measured by using an EOL JEM-1011 transmission electron microscope (TEM). The size distribution and zeta potential of LPs were determined by dynamic light scatting analysis (DLS, Malvern Nano ZS90, UK). The absorbance and fluorescence spectra of liposomes were obtained using an ultraviolet−visible spectrometer (UV−Vis, UV-2450PC, Shimadzu, Japan) and fluorescence Spectrometer (LS50B, PerkinElmer, USA), respectively.

To determinate the lipid peroxidation, the formation of conjugated dienes was assessed by spectrophotometry. The photo-triggered lipid peroxidation reaction was measured in both ethanol, where the lipid and Ce6 were dispersed, and in PBS, where Ce6 was encapsulated in the lipid bilayer (TP/Ce6-LP). The solution was irradiated at 650 nm, 0.5 W/cm2, and the absorption at 200−300 nm was monitored.

To determine the release profile of TP, the TP/Ce6-LP solutions were first treated under different conditions: 1) 650 nm NIR irradiation at a power density of 0.5 W cm-2 for 5 min, 2) 100 μmol/L of H2O2, and 3) PBS solution. Then, the solution was transferred into a dialysis bag (MWCO = 3500 Da) placed in 100 mL related release medium at 37 °C under constant shaking. At indicated time points, 2 mL of release medium was removed for further measurement, followed by the addition of 2 mL release medium to keep the total volume constant. The amount of released TP was measured by using HPLC.

2.4. *Singlet oxygen generation*

Singlet oxygen generation of photo-triggered liposome *in vitro* was measured by DPBF(1,3-diphenylisobenzofuran). The TP/

Ce6-LP with or without VC mixture were mixed with 20 μmol/L DPBF, followed by 3 min irradiation with a power intensity (650 nm laser, 0.5 W/cm2). The absorbance of DPBF at 415 nm was monitored during the irradiation. Singlet oxygen generation of photo-triggered liposome in cells was measured by 2′,7′-dichlorodihydrofluorescein diacetate (DCFH-DA). HepG2 cells were seeded in 6-well plates and cultured for 12 h, followed by treatment with TP/Ce6-LP at a Ce6 concentration of 5 μmol/L for 4 h. Then, the TP/Ce6-LP were divided into two parts, which were exposed under 3 min irradiation (650 nm laser, 0.5 W/cm2) or without irradiation.

2.5. *Cellular uptake*

HepG2 cells (5×10^5) were seeded in 6-well plates in 1640 medium and cultured for 12 h. After treated with PBS for 8 h, Ce6 for 8 h, TP/Ce6-LP for 2, 4, and 8 h, respectively, the cells were fixed with 4% (*w*/*v*) paraformaldehyde for 30 min. Then, the cell nucleus was stained with DAPI (blue) for 5 min. Next, the actin cytoskeleton of cells was stained with FITC phalloidin (green) for 30 min. Last, the cells were visualized under confocal laser scanning microscopy (CLSM). For flow cytometry study, HepG2 cells (2×105) were seeded in 6-well plates in 1640 medium and

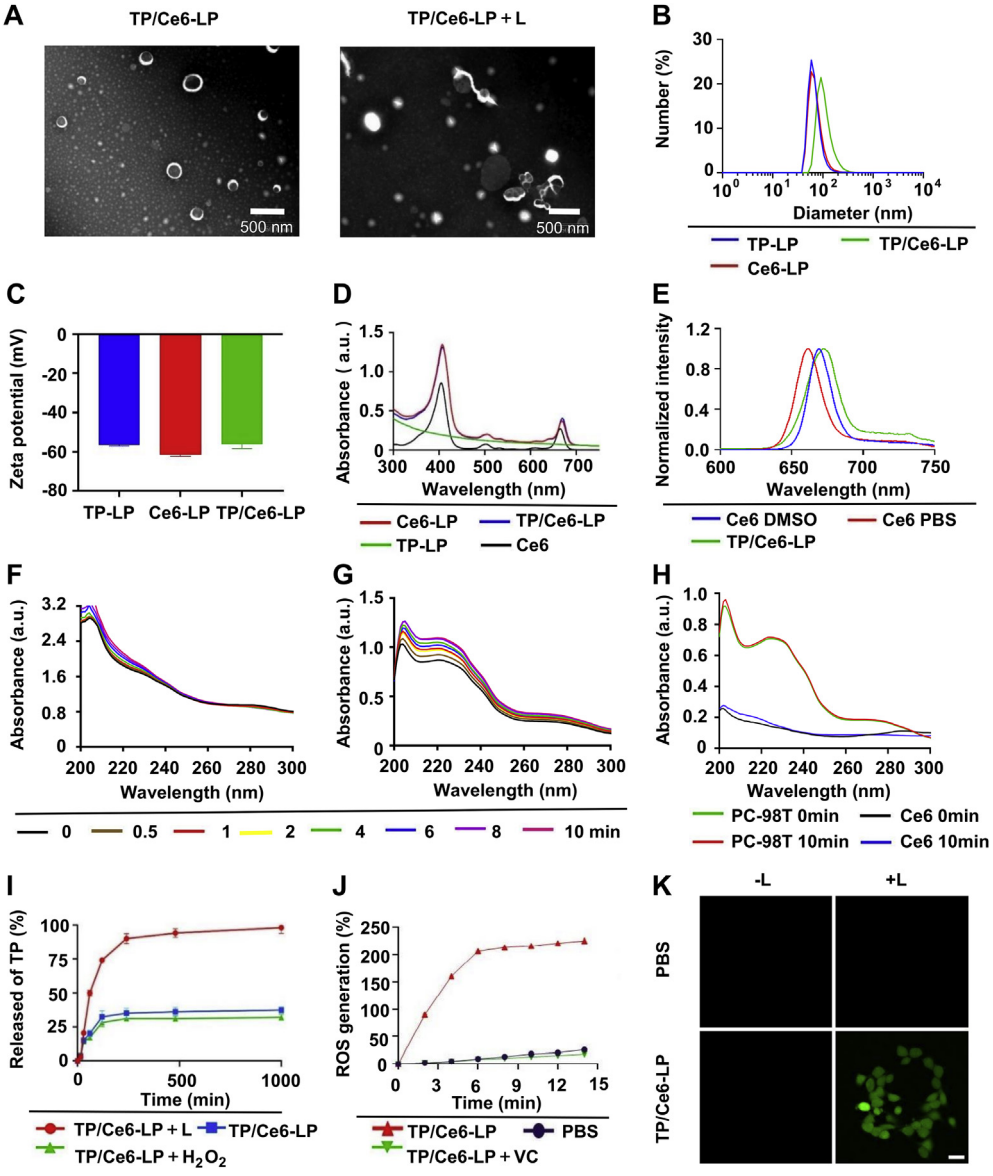

Figure 1 Characterization of photosensitive liposomes. (A) TEM images of TP/Ce6-LP and coalescent TP/Ce6-LP after 3 min irradiation (650 nm, 0.5 W/cm^2). Size distribution(B) and Zeta potential (C) of TP-LP, Ce6-LP and TP/Ce-LP, data are expressed as median, $n = 3$. (D) UV−Vis spectra of TP-LP, Ce6-LP, TP/Ce-LP and free Ce6. (E) Fluorescence spectra of Ce6 in DMSO, Ce6 in PBS and TP/Ce6-LP. UV−Vis spectra of TP/Ce6-LP (F) and PC-98T and Ce6 mixture (G) after 0, 0.5, 1, 2, 4, 6, 8, 10 min laser irradiation. (H) UV−Vis spectra of separate PC-98T solution and Ce6 solution after 0 and 10 min laser irradiation. (I) Release profile of TP from TP/Ce6-LP with or without periodic irradiation (650 nm, 0.5 W/cm2) and treatment with H2O2 (100 μmol/L). Data are presented as mean ± SD, $n = 3$. (J) ROS generation measurements by DPBF assay with or without laser irradiation (650 nm, 0.5 W/cm2). (K) ROS generation in HepG2 cells measured by CLSM. Scale bar = 20 μm.

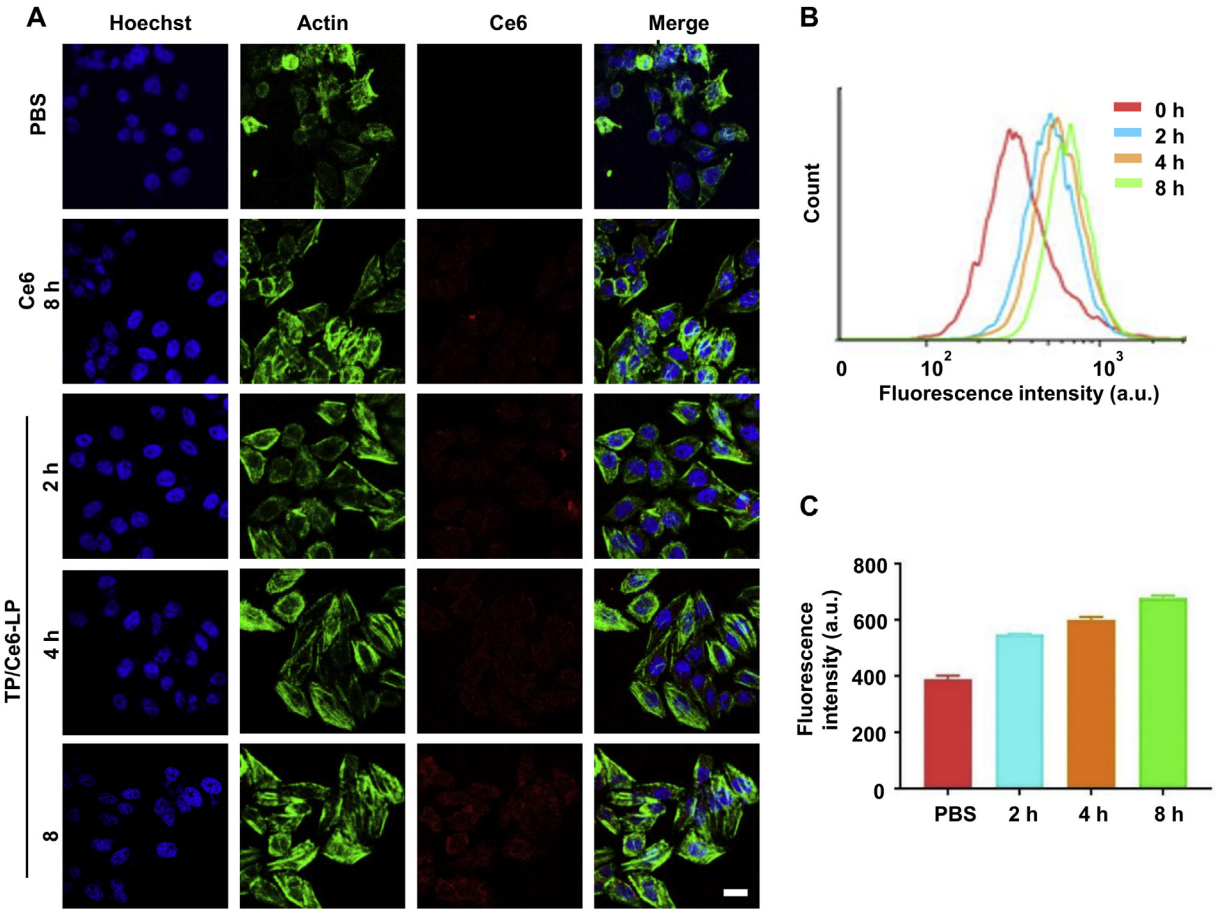

Figure 2 *In vitro* intracellular uptake. (A) CLSM of HepG2 cells after incubation with PBS for 8 h, Ce6 for 8 h, TP/Ce6-LP for 2, 4, and 8 h. The cell nucleus was stained by Hoechst 33342, The actin cytoskeleton was stained by Phalloidin FITC. Scale bar = 20 μm. Flow cytometry (B) statistics (C) of HepG2 cells after treated with TP/Ce6-LP for 2, 4, 8 h. Data are presented as mean ± SD (n = 3).

cultured for 12 h. Then the cells were treated with TP/Ce6-LP (Ce6 concentration: 5 μmol/L) at 37 °C for 2, 4 and 8 h, respectively. The collected cells were resuspended with PBS for detection by Flow Cytometry (FCM).

2.6. *Cell viability studies*

HepG2 cells (5×10^3) and 7404 cells (5×10^3) were seeded in 96-well plates in 1640 medium and cultured for 12 h. The medium was replaced with culture medium with the following drugs: TP/Ce6-LP+L, P/Ce6-LP-L, TP-LP+L, TP-LP-L, Ce6-LP+L, triptolide (TP), platinum (Pt), sorafenib (So), doxorubicin (Dox) at the concentration from 0.00625 to 50 μmol/L. After incubating for 24 h, the TP/Ce6-LP, TP-LP and Ce6-LP were irradiated with 650 nm light for 3 min. After 24 h incubation, 5 mg/mL MTT solution in PBS was added and the plates were incubated for another 4 h at 37 °C. Followed by slightly removal of the culture medium containing MTT, 150 μL of dimethyl sulfoxide (DMSO) was added to each well. Finally, the absorbance of the above solution was measured on a microplate reader (Infinite M1000 Pro, Tecan, Switzerland) at 490 nm.

2.7. *Apoptosis analysis*

HepG2 cells (5×10^5) were seeded in 6-well plates in 1640 medium and cultured for 12 h. After treated with the fresh medium with TP/Ce6-LP+L, Ce6-LP-L, TP-LP+L, TP-LP-L, Ce6-LP+L, TP, Pt, So, Dox for 12 h, the TP/Ce6-LP+L, TP-LP+L and Ce6-LP+L groups were irradiated with light at 650 nm (3 min). The cells were incubated another 12 h after irradiation and harvested to stain with annexin-V FITC and PI according to the manufacturer's protocol for flow cytometry. Then the data were analyzed with FlowJo software.

2.8. *Tissue distribution*

BALB/c nude mice (18−20 g) were purchased from Guangdong Medical Laboratory Animal Center (Guangdong, China). All animal studies were carried out under Institutional Animal Care and Use Committee approved protocols of Southern Medical University. For *in vivo* fluorescence imaging, the subcutaneous patient-derived xenograft (PDX) model of HCC was established. When the tumor size reached of 150 mm^3, mice were intravenously injected with free Ce6 and TP/Ce6-LP. The photos were taken at 4, 8 and 24 h after the drug injection. *In vivo* fluorescence imaging was performed on an IVIS Lumina III Imaging System (Caliper, USA) with excitation filter of 670 nm and emission filter of 700−800 nm. After the mice were sacrificed, tumor and tissues were excised and subjected to *ex vivo* fluorescence imaging and tissue section staining.

2.9. *In vivo anticancer efficacy*

PDX tumor-bearing mice established as described above were randomly divided into PBS, So, TP, Ce6-LP+L, TP/Ce6-LP-L and TP/Ce6-LP+L groups ($n = 5$). At Days 0, 2, 4, and 6, the mice were administered intravenously with drugs at the 10 mg/kg dose of So, 0.04 mg/kg dose of Ce6 and 0.4 mg/kg dose of TP. Ce6-LP+L and TP/Ce6-LP+L groups were irradiated with light at 650 nm (0.5 W/cm2, 10 min) at Days 1, 3, 5 and 7. Tumor length (L) and width (W) were measured with calipers every day, and the tumor volume (V, mm3) was calculated. The body weight of each group was monitored every day as an indicator of systemic toxicity. The mice were sacrificed after therapeutic experiments and the tumors were weighted. The blood of mice was collected by eyeball blood collection method. Then tumors and major organs including heart, liver, spleen, lung, kidney were collected and kept in 4% (w/v) paraformaldehyde overnight for hematoxylin and eosin (H&E) staining, terminal deoxynucleotidyl transferase-mediated dUTP-biotin nick end labeling (TUNEL) assay. In addition, the fresh tumors excised from mice were prepared for Western blotting.

2.10. *Western blotting*

Total proteins were extracted from tumor tissues. BCA protein assay kit was used to determine the protein concentration of each sample. Then equal amount protein samples were scraped into SDS-PAGE gel electrophoresis, followed by electro-transferring to PVDF membrane. These membranes were incubated with the primary antibodies at 4 °C overnight and horseradish peroxidase-conjugated secondary antibodies for 2 h. The immune complexes of each group were detected by ECL western blotting detection system.

2.11. *Detection of blood biochemical indexes*

The blood sample of mice was collected and centrifuged at 5000 rpm (Eppendorf Centrifuge 5424) for 5 min to obtain plasma samples for measuring the clinic parameters including heart indices containing creatine kinase (CK), creatine kinase-MB (CK-MB), and lactate dehydrogenase (LDH), liver-related alanine aminotransferase (ALT) and aspartate aminotransferase (AST),

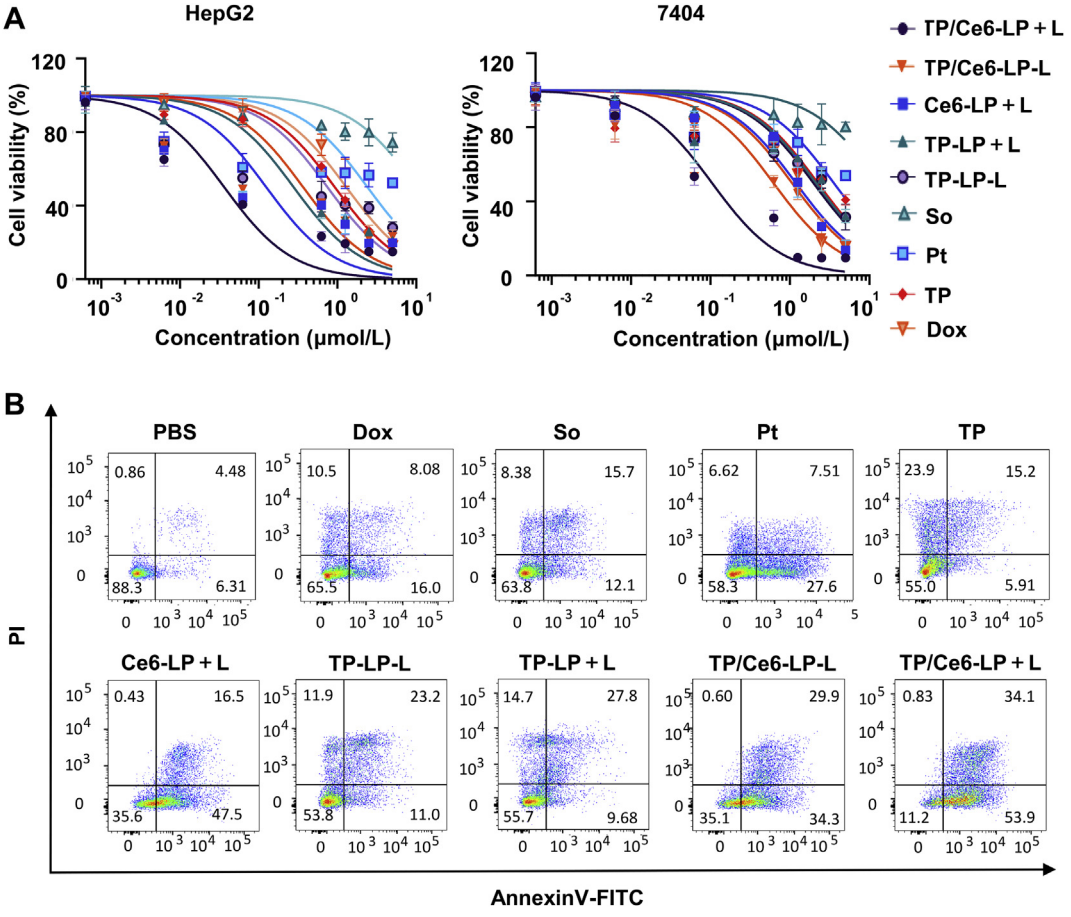

Figure 3 *In vitro* evaluation of anticancer activity. (A) Relative cell viability of HepG2 and 7404 cells after 48 h incubation of TP/Ce6-LP+L, TP/Ce6-LP-L, TP-LP+L, TP-LP-L, Ce6-LP+L, Triptolide (TP), Cisplatin (Pt), Sorafenib (So), Doxorubicin (Dox). (B) The Annexin-V/PI apoptosis assay of HepG2 cells after treated with each group for 24 h measured by FCM analysis.

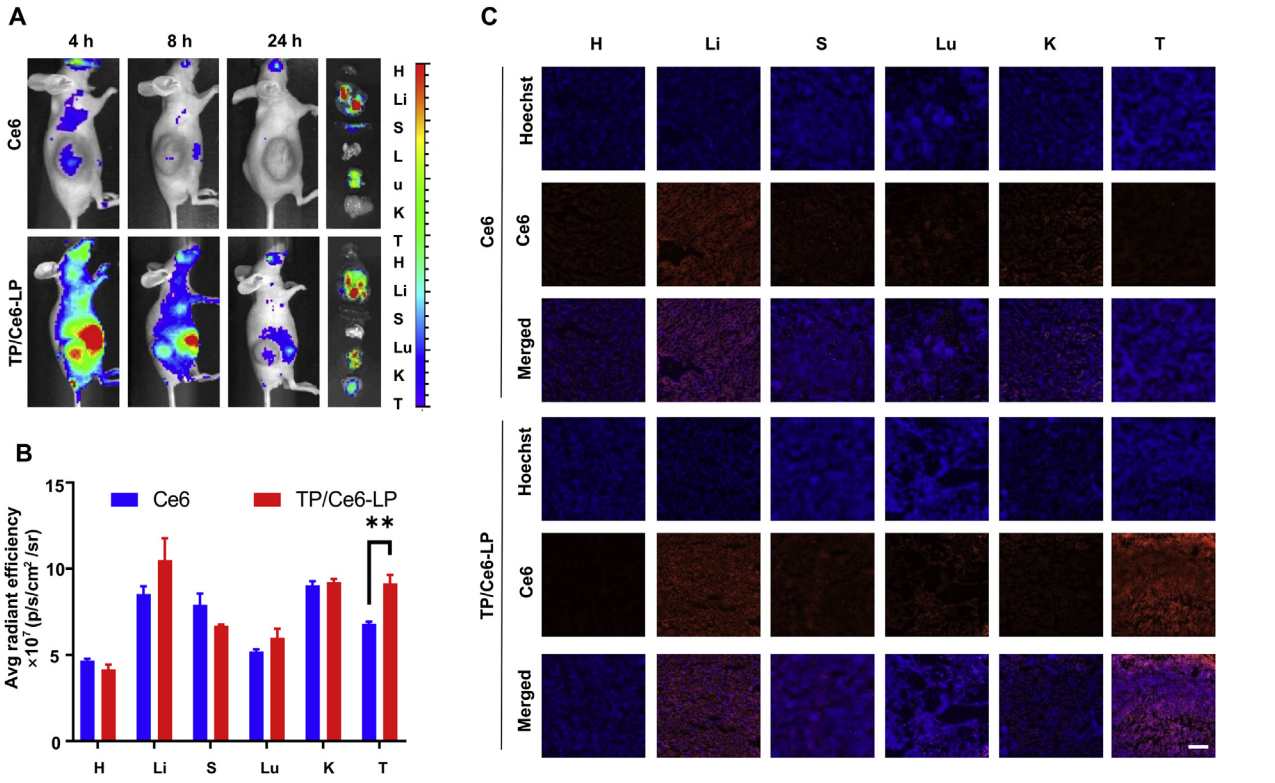

Figure 4 Tumor imaging and biodistribution of Ce6 and TP/Ce6-LP. (A) *In vivo* images after treatment with Ce6 or TP/Ce6-LP at different time and the e*x vivo* images of Heart (H), Liver (Li), Spleen (S), Lung (Lu), Kidney (K), Tumor (T) separated from mice at 24 h post injection. (B) Mean fluorescence intensity of normal tissues and tumors. (C) The distribution in tissue slices after injection of Ce6 or TP/Ce6-LP for 24 h, cell nucleus was stained by Hoechst 33342. Data are presented as mean ± SD ($n = 3$). Scale bar = 100 μm.

and kidney-associated blood urea nitrogen (BUN) and creatinine (Cr) by an automatic biochemical analyzer.

2.12. *Statistical analysis*

The experimental data expressed as mean ± SD was analyzed using one-factor analysis of variance (SPSS software, version 22.0, SPSS Inc.). Statistical difference between various experimental and control groups was analyzed by Student's *t*-test or ANOVA analysis. Differences were considered statistically significant at a level: $^{*}P < 0.05$, $^{**}P < 0.01$ and $^{***}P < 0.001$.

3. Results

3.1. *Preparation and characterization of TP/Ce6-LP*

The lipid film Ce6 and TP were hydrated with aqueous solution to prepare photo-sensitive liposome (LP). The drug encapsulation efficiency (DEE) of TP was 22.4% (TP-LP) and 26.7% (TP/Ce6-LP). The DEE of Ce6 was 91.7%. The drug-loading content (DLC) of TP was estimated to be 3.0% (TP-LP) and 3.6% (TP/Ce6-LP, *w/w*). The DLC of Ce6 was estimated to be 0.18%. The hydrodynamic diameters of TP-LP, Ce6-LP and TP/Ce6-LP were measured as 71.22, 72.88, and 109.97 nm by dynamic light scattering (DLS, Fig. 1B). Concurrently, the zeta potential of these three liposomes were determined as −56.67, −61.47 and −56.33 mV (Fig. 1C). We examined the morphology of TP/Ce6-LP before and after the laser irradiation by transmission electron microscopy (TEM, Fig. 1A). According to the TEM, TP/Ce6-LP possessed the spherical structure. TP/Ce6-LP is oxidized and their structural integrity was destroyed after laser irradiation. The absorption and fluorescent spectra of TP/Ce6-LP and Ce6-LP indicated that Ce6 were successfully encapsulated in the liposomes, verifying that the near infrared emissions from TP/Ce6-LP could motivate the PDT process and trigger the release of TP (Fig. 1D and E). The peroxidation of unsaturated phospholipids experiment has been assessed by following the absorption spectra. Upon irradiation of Liposomes, the absorption peak at 238 nm increased with time, indicating the occurrence of lipid peroxidation (Fig. 1F). Irradiation of PC-98T and Ce6 mixture also has the above phenomenon (Fig. 1G). However, when PC-98T and Ce6 were irradiated, respectively, there were negligible changes at 238 nm (Fig. 1H) These results proved that peroxidation of unsaturated phospholipids was triggered by the NIR-induced ROS.

To demonstrate the light-responsive behavior of TP/Ce6-LP, the drug release of TP was conducted in dark or under NIR irradiation and with 100 μmol/L H2O2 (Fig. 1I). Results show that TP/Ce6-LP exhibited a sustained release and limited TP release in the absence of NIR light as well as in H2O2 (37% and 32% of TP released) at 1000 min. Under NIR irradiation, 98% of TP was rapidly released from nanoparticles in 1000 min. These results show that liposomes could be released under light irradiation. To confirm the ROS generation that could trigger the oxidation of unsaturated phospholipid under irradiation, the *in vitro* generation of singlet oxygen was evaluated by DPBF. We observed that ROS production increased rapidly over an irradiation time in 6 min (Fig. 1J). To further confirm the ROS generation can be possible in cells, *in situ* ROS production in HepG2 cells was measured by DCFH-DA using CLSM (Fig. 1K). Results demonstrate that HepG2 cells treated with TP/Ce6-LP follow by irradiation produced more ROS than other treatment group.

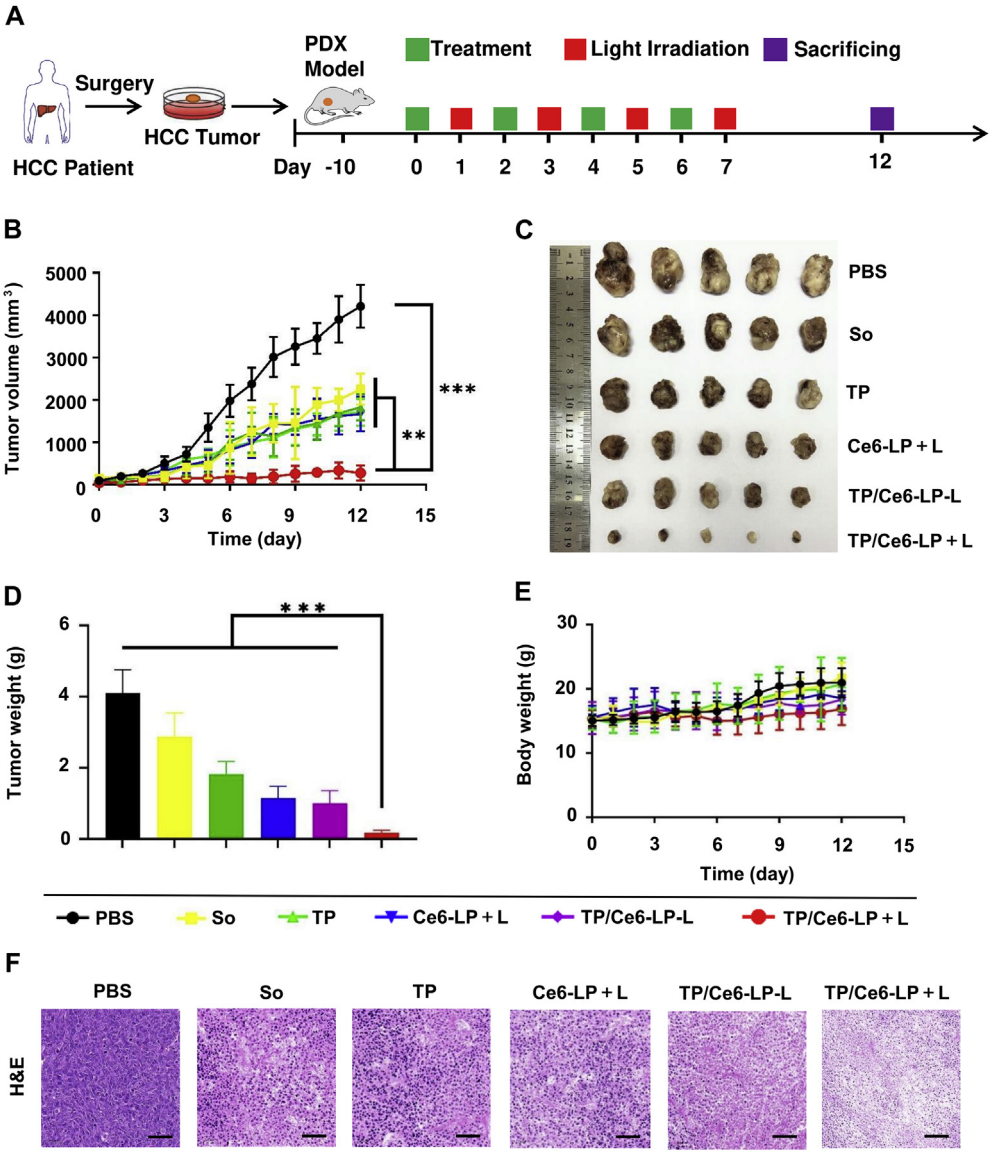

Figure 5 *In vivo* antitumor efficacy. (A) Schematic illustration of therapeutic scheme on PDX model. (B) Tumor growth inhibition curves of mice after intravenous injection of different formulations ($n = 5$). (C) Photos of tumors. (D) The weight of tumors. (E) Body weight of mice during treatment. (F) H&E staining of tumor tissues. Data are presented as mean ± SD, $n = 5$; $^{**}P < 0.01$, $^{***}P < 0.001$. Scale bar = 50 μm.

3.2. *Cellular uptake of TP/Ce6-LP*

As Ce6 is fluorescent, Ce6 fluorescence was applied to track the internalization of nanoparticles *via* CLSM and FCM in HepG2 cells. TP/Ce6-LP entered tumor cells through an endocytosis pathway, leading to the intercellular accumulation of drugs for promoting the drug uptake. The results showed a time-dependent increase in TP/Ce6-LP uptake on the HepG2 cells for different time points (Fig. 2A). In addition, TP/Ce6-LP achieved remarkable higher drug uptake than free Ce6. Further quantitative results by flow cytometry also showed that the fluorescence intensity in HepG2 cells increased 1.7-fold after 8 h treatment with TP/Ce6-LP than cells in PBS (Fig. 2B and C).

3.3. *Proliferation inhibition*

The cytotoxicity of TP/Ce6-LP in comparison to various agents was evaluated by MTT assay on HepG2 and 7404 cells under light irradiation or without light irradiation (Fig. 3A). Upon 650 nm light irradiation, the cell viability of TP/Ce6-LP decreased with the increase of TP concentration, exhibiting the most remarkable effect to kill cancer cells compared with free TP. This synergy also confirmed by cell apoptosis evaluation. Determination of the apoptosis on HepG2 cells incubated with the same experimental and control agents showed similar trends of MTT results (Fig. 3B). TP/Ce6-LP followed by NIR irradiation (75% cell apoptosis) significantly increased cell death compared with TP (36% cell

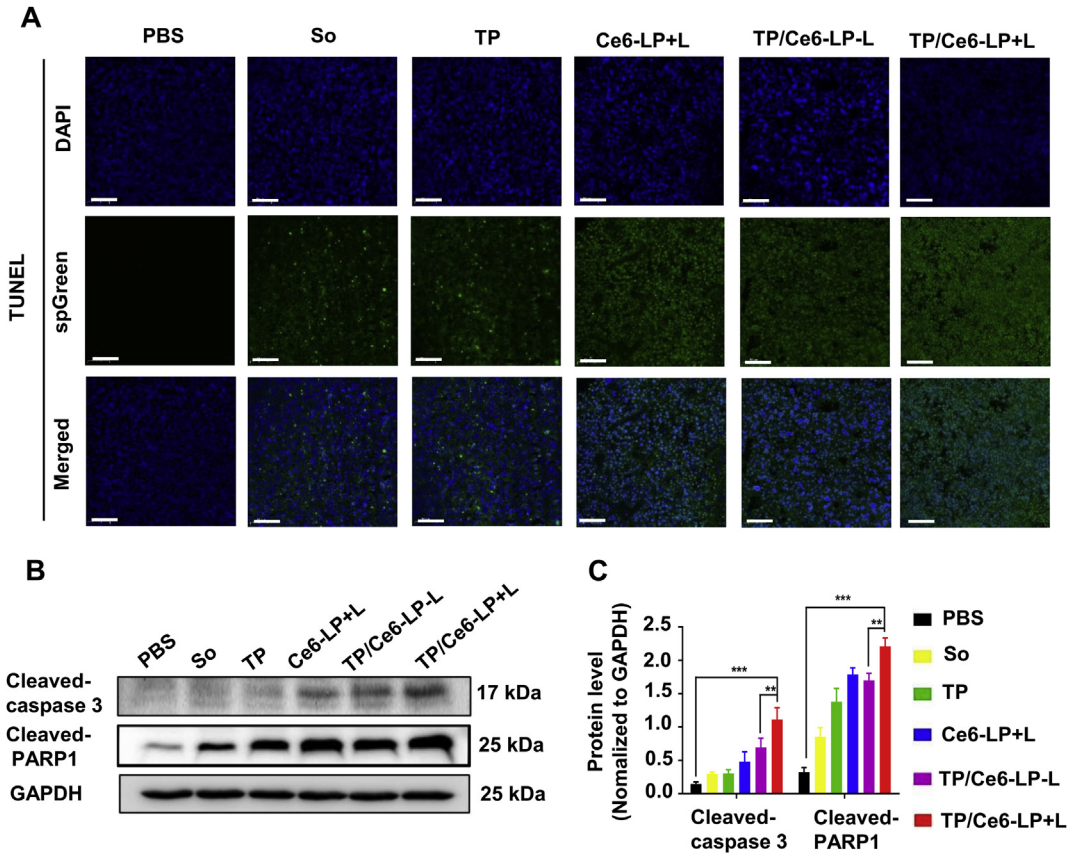

Figure 6 Molecular mechanism of light-activatable synergistic therapy. (A) TUNEL staining of tumor tissues. Scale bar: 50 μm. Western blotting (B) and the quantification analysis (C) of Cleaved Caspase 3 and Cleaved-PARP1. Data are presented as mean ± SD, $n = 3$; $^{**}P < 0.01$, $^{***}P < 0.001$.

apoptosis), confirming that TP/Ce6-LP possessed excellent therapeutic effect.

3.4. *Biodistribution study*

Improved accumulation in tumor is critical for the ultimate therapeutic consequence. The biodistribution of TP/Ce6-LP and Ce6 in BABL/c nude mice bearing PDX model of hepatocellular carcinoma was determined by real-time IVIS imaging. The Ce6 fluorescence appeared to persist in tumors despite 24 h post administration in TP/Ce6-LP group, but in Ce6 group it has disappeared (Fig. 4A). *Ex vivo* imaging and semi-quantitative analysis for the major organs also suggested that TP/Ce6-LP had markedly stronger fluorescence compared to Ce6 (Fig. 4B). After 24 h administration, the isolated organs and tumor tissues were stained to observe the drug distribution. The results find that the fluorescence intensity of TP/Ce6-LP group was much higher than that of Ce6 group in the tumor site (Fig. 4C). These results show that TP/Ce6-LP possess appreciable tumor accumulation and retention for a wide treatment window.

3.5. *Antitumor efficacy on PDX model of HCC*

Free drug and drug-loading photo-activatable liposomes were tested on BALB/c nude mice bearing PDX model of hepatocellular carcinoma to explore the advantages of drug releasing platform for tumor. Herein, when the tumor volume reached about 50 mm^3, the mice were treated with diverse therapeutic groups (Fig. 5A). Compared with PBS group, So, TP, Ce6-LP+L and TP/Ce6-LP-L groups have some anti-tumor effects. However, TP/Ce6-LP+L exhibited best antitumor effect, which significantly inhibited the tumor volume to 276 mm^3 after 12 day (Fig. 5B and C). In addition, the tumor weight in TP/Ce6-LP+L group was only 4% of the PBS group, which showed the significant tumor suppression (Fig. 5D). During the treatment period, all groups showed no obvious weight loss, indicating that our photo-activatable liposomes had good biocompatibility (Fig. 5E). These data demonstrate that TP delivered by the adjustable photo-activatable liposome dominated the synergistic therapy and show great therapeutic advantages in HCC tumor. In addition, TP/Ce6-LP+L group displayed much better antitumor effect than PBS group according to the significant histological damages in the tumor sections validated by the hematoxylin and eosin (H&E, Fig. 5F), consisting with the above *in vivo* antitumor effects.

3.6. *Molecular mechanism of photo-activatable synergistic therapy*

The potent anti-tumor efficacy of TP/Ce6-LP was further validated by TdT-mediated dUTP Nick-End Labeling (TUNEL)-staining of tumor tissue sections (Fig. 6A). It was found that the degree of apoptosis in PBS group was lower, while that in TP/Ce6-LP+L group was the highest and the relative level appeared in the following order: PBS<So< TP<Ce6-LP+L<TP/Ce6-LP-L<TP/Ce6-LP+L. Further Western blotting quantification analysis after treatment with each group were also performed (Fig. 6B and C). These results show that TP/Ce6-LP+L produced more

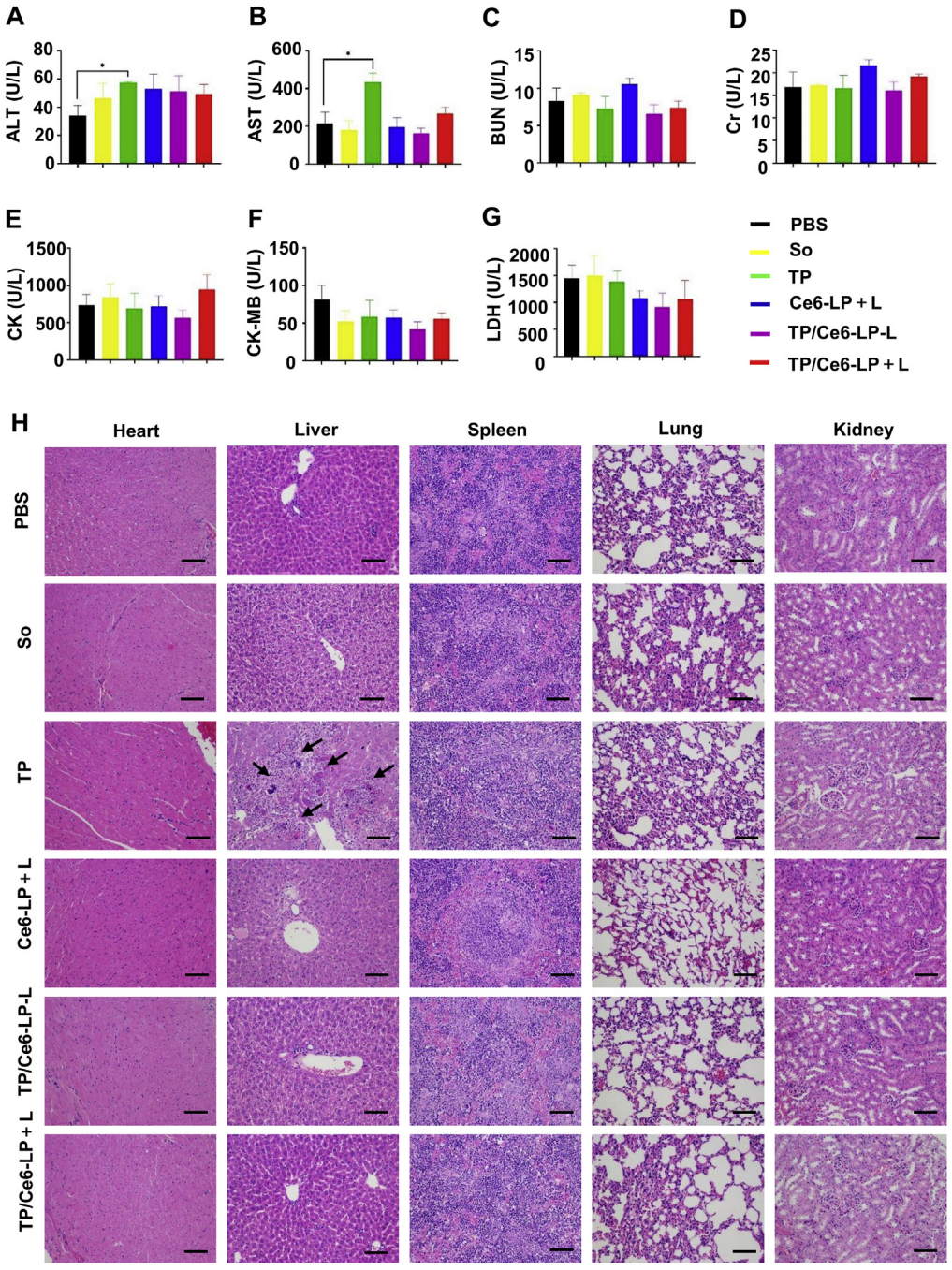

Figure 7 *In vivo* systemic toxicities study. Evaluations of ALT (A) AST (B) BUN (C) Cr (D) CK (E) CK-MB (F) and HDL-L (G) in female BALB/c mice after treatments with PBS, So, TP, Ce6-LP+L, TP/Ce6-LP-L and TP/Ce6-LP+L. (H) Histological analysis of main organs from PDX model of HCC after treatment with corresponding groups. Data are presented as mean ± SD, $n = 5$; $^*P < 0.05$. Scale bar: 50 μm.

CLEAVED CASPASE-3 in tumor tissue, and the relative level appeared in the following order: PBS<So<TP<Ce6-LP+L<TP/Ce6-LP-L<TP/Ce6-LP+L. CLEAVED-PARP1 expression was in the same order, suggesting that TP/Ce6-LP induced cell apoptosis through increasing CLEAVED CASPASE-3 and CLEAVED-PARP1 expression.

3.7. *Application safety evaluation*

The blood biochemistry analysis (Fig. 7A–G) on the BALB/c mice and H&E examination of the normal organs (Fig. 7H) collected from mice receiving different treatments for 12 d were determined for evaluation of application safety. There were no

obvious changes in major organs after treatment with drug-loading liposomes, verifying an excellent biocompatibility. However, the blood liver function indexes (ALT and AST) of TP group were higher than that of PBS group, indicating that TP induced liver function injury. Moreover, H&E staining pictures of liver in TP group showed scattered apoptotic bodies, round apoptotic cells, deep nuclear staining and cytoplasmic condensation, indicating that TP was harmful to the liver. These results demonstrated that drug-loading liposomes reduced side effects of TP.

4. Discussion

HCC has unfavorable prognosis for survival as it is poorly responsive to current therapy[1,36]. At present, the main chemotherapeutic agent clinically used in the treatment of HCC is sorafenib. Sorafenib is included in the clinical treatment of HCC as the first-line agent in 2008, owing to effective suppression effect of both tumor cell proliferation and tumor angiogenesis. However, with nonspecific distribution *in vivo* and insufficient dosage in the tumor site, sorafenib can only increase average survival by two months, which resulting in its highly restricted clinically[37]. TP has been considered to be a more promising therapeutic agent against HCC than sorafenib[38]. However, its high toxicity and poor solubility limit its clinical application[16]. Thus, reducing the side effects and improving therapeutic index of TP should be the direction of our efforts in the treatment of HCC.

Nanomedicine derived from nano-size drug delivery systems has significantly improved drug delivery to specific cells or tissues, including stimuli-responsive nanoparticles[18,24]. Growing evidence shows that stimuli-responsive nanoparticles have considered as a drug delivery system for targeted intracellular controlled release delivery of chemotherapeutic agents[24,39]. Currently, it has attracted more attention for clinical therapy[40]. Therefore, we synthesized a photo-activatable liposomes integrated Ce6 and TP (TP/Ce6-LP) for HCC targeted therapy. The TP/Ce6-LP+L systems were characterized by excellent stability, improved tumor accumulation, desirable endocytosis, as well as preferable drug release capacity, which also verified by drug particle size stability test, drug release test, cell endocytosis test[13,41].

In our study, we have observed that TP/Ce6-LP+L has stronger anti-HCC efficacy than free TP *in vivo*. This result is probably due to several advantages of TP/Ce6-LP+L. Firstly, as compared to normal tissues, TP/Ce6-LP+L improved tumor accumulation through the EPR effect, resulting in a stronger anti-HCC efficacy. Secondly, with NIR irradiation, ROS is released by photosensitizers (Ce6) within TP/Ce6-LP. Thirdly, the released ROS plays a direct role in the process of photodynamic therapy (PDT). Fourthly, the allylic hydrogen structure in unsaturated phospholipid reversibly formed hydrophilic lipid peroxides upon intermittent near-infrared light-induced ROS, thus facilitating on-demand release of TP prodrugs from liposomes to enter the tumor cells. Last but not the least, the toxicity of TP was notably reduced following its encapsulation in TP/Ce6-LP. Taken together, TP/Ce6-LP+L achieved ON/OFF drug release, thereby reducing tumor sizes in PDX model, suggesting its targeting and control potential. Furthermore, in order to clarify its molecular mechanism, the whole lysate was extracted from tumor tissues for Western blot assay. More interestingly, cleaved-caspase-3 and cleaved-PARP1 were markedly up-regulated in PBS group, while tumor treated with TP/Ce6-LP+L had the highest protein levels. These results demonstrate that TP/Ce6-LP+L mediated apoptosis through caspase-3/PARP signaling.

5. Conclusions

In summary, a preferable photo-activatable drug release capacity liposome carrying Ce6 and TP for synergistic PDT and chemotherapy for HCC treatment was developed. The ROS generated in PDT commits oxidization of the unsaturated phospholipid in liposome, enabling light-triggered TP release from liposomes. TP/Ce6-LP has high cytotoxicity and excellent anti-tumor effect on the PDX model of HCC, TP/Ce6-LP increased cell apoptosis through increasing cleaved-caspase-3 and cleaved-PARP1 expression. In addition, TP/Ce6-LP reduced the hepatotoxicity of TP, demonstrating good biocompatibility. In short, TP/Ce6-LP is a novel potential treatment option in halting HCC progression with attenuate toxicity.

Acknowledgments

This study was supported by China postdoctoral Science Foundation (No. 2020M673026), the National Natural Science Foundation of China (Nos. 81873248, 81673903 and 81773642), Opening Project of Zhejiang Provincial Preponderant and Characteristic Subject of Key University (Traditional Chinese Pharmacology, China), Zhejiang Chinese Medical University (No. ZYAOXZ2018014, China), and State Key Laboratory of Molecular Engineering of Polymers (2019–06, Fudan University, China).

Author contributions

Zhiqiang Yu and Shijun Zhang designed the research. Ling Yu carried out the experiments and performed data analysis. Zhenjie Wang, Zhuomao Mo and Binhua Zou participated part of the experiments. Yuanyuan Yang, Rui Sun and Wen Ma provided experimental drugs and quality control. Ling Yu and Zhenjie Wang wrote the manuscript. Meng Yu and Zhiqiang Yu revised the manuscript. All of the authors have read and approved the final manuscript.

Conflicts of interest

The authors have no conflicts of interest to declare.

References

1. Müller M, Bird TG, Nault JC. The landscape of gene mutations in cirrhosis and hepatocellular carcinoma. *J Hepatol* 2020;**72**:990−1002.
2. Dimitroulis D, Damaskos C, Valsami S, Davakis S, Garmpis N, Spartalis E, et al. From diagnosis to treatment of hepatocellular carcinoma: an epidemic problem for both developed and developing world. *World J Gastroenterol* 2017;**23**:5282−94.
3. Hassanipour S, Vali M, Gaffari-Fam S, Nikbakht HA, Abdzadeh E, Joukar F, et al. The survival rate of hepatocellular carcinoma in Asian countries: a systematic review and meta-analysis. *EXCLI J* 2020;**19**:108−30.
4. Sun Y, Ma W, Yang Y, He M, Li A, Bai L, et al. Cancer nanotechnology: enhancing tumor cell response to chemotherapy for hepatocellular carcinoma therapy. *Asian J Pharm Sci* 2019;**14**:581−94.
5. Duan X, Chan C, Han W, Guo N, Weichselbaum RR, Lin W. Immunostimulatory nanomedicines synergize with checkpoint

blockade immunotherapy to eradicate colorectal tumors. *Nat Commun* 2019;**10**:1899.
6. Nault J-C, Villanueva A. Biomarkers for hepatobiliary cancers. *Hepatology* 2021;**73S1**:115−27.
7. Avila MA, Berasain C, Sangro B, Prieto J. New therapies for hepatocellular carcinoma. *Oncogene* 2006;**25**:3866−84.
8. Cheng AL, Kang YK, Chen Z, Tsao CJ, Qin S, Kim JS, et al. Efficacy and safety of sorafenib in patients in the Asia-Pacific region with advanced hepatocellular carcinoma: a phase III randomised, double-blind, placebo-controlled trial. *Lancet Oncol* 2009;**10**:25−34.
9. Yang C, Xing L, Chang X, Zhou T, Bi Y, Yu Z, et al. Synergistic platinum(II) prodrug nanoparticles for enhanced breast cancer therapy. *Mol Pharm* 2020;**17**:1300−9.
10. Satpathy M, Wang L, Zielinski RJ, Qian W, Wang YA, Mohs AM, et al. Targeted drug delivery and image-guided therapy of heterogeneous ovarian cancer using HER2-targeted theranostic nanoparticles. *Theranostics* 2019;**9**:778−95.
11. Liu Q. Triptolide and its expanding multiple pharmacological functions. *Int Immunopharm* 2011;**11**:377−83.
12. Zhao X, Liu X, Zhang P, Liu Y, Li Y. Injectable peptide hydrogel as intraperitoneal triptolide depot for the treatment of orthotopic hepatocellular carcinoma. *Acta Pharm Sin B* 2019;**9**:1050−60.
13. Zhang YQ, Shen Y, Liao MM, Mao X, Mi GJ, You C, et al. Galactosylated chitosan triptolide nanoparticles for overcoming hepatocellular carcinoma: enhanced therapeutic efficacy, low toxicity, and validated network regulatory mechanisms. *Nanomed Nanotechnol* 2019;**15**:86−97.
14. Liu M, Song W, Du X, Su J, Dong K, Chen Y, et al. NQO1-selective activated prodrug of triptolide: synthesis and anti-hepatocellular carcinoma activity evaluation. *ACS Med Chem Lett* 2018;**9**:1253−7.
15. Yuan Z, Yuan Z, Hasnat M, Zhang H, Liang P, Sun L, et al. A new perspective of triptolide-associated hepatotoxicity: the relevance of NF-κB and NF-κB-mediated cellular FLICE-inhibitory protein. *Acta Pharm Sin B* 2020;**10**:861−77.
16. Zhou ZL, Yang YX, Ding J, Li YC, Miao ZH. Triptolide: structural modifications, structure–activity relationships, bioactivities, clinical development and mechanisms. *Nat Prod Rep* 2012;**29**:457−75.
17. Zhao X, Liu X, Zhang P, Liu Y, Ran W, Cai Y, et al. Injectable peptide hydrogel as intraperitoneal triptolide depot for the treatment of orthotopic hepatocellular carcinoma. *Acta Pharm Sin B* 2019;**9**:1050−60.
18. Qiao Y, Wan J, Zhou L, Ma W, Yang Y, Luo W, et al. Stimuli-responsive nanotherapeutics for precision drug delivery and cancer therapy. *WIREs Nanomed Nanobi* 2019;**11**:e1527.
19. Yang Y, Chen Q, Lin J, Cai Z, Liao G, Wang K, et al. Recent advance in polymer based microspheric systems for controlled protein and peptide delivery. *Curr Med Chem* 2019;**26**:2285−96.
20. Chen Q, Yang Y, Lin X, Ma W, Chen G, Li W, et al. Platinum(IV) prodrugs with long lipid chains for drug delivery and overcoming cisplatin resistance. *Chem Commun* 2018;**54**:5369−72.
21. Huang P, Wang G, Su Y, Zhou Y, Huang W, Zhang R, et al. Stimuli-responsive nanodrug self-assembled from amphiphilic drug–inhibitor conjugate for overcoming multidrug resistance in cancer treatment. *Theranostics* 2019;**9**:5755−68.
22. Chen Z, Wu C, Zhang Z, Wu W, Wang X, Yu Z. Synthesis, functionalization, and nanomedical applications of functional magnetic nanoparticles. *Chin Chem Lett* 2018;**29**:1601−8.
23. Preiss MR, Bothun GD. Stimuli-responsive liposome-nanoparticle assemblies. *Expet Opin Drug Deliv* 2011;**8**:1025−40.
24. Li Z, Yin Y. Stimuli-responsive optical nanomaterials. *Adv Mater* 2019;**31**:e1807061.
25. Sun Y, Zhan A, Zhou S, Kuang X, Shen H, Liu H, et al. A novel mitochondria-targeting tetrapeptide for subcellular delivery of nanoparticles. *Chin Chem Lett* 2019;**30**:1435−9.
26. Xiao H, Yan L, Dempsey EM, Song W, Qi R, Li W, et al. Recent progress in polymer-based platinum drug delivery systems. *Prog Polym Sci* 2018;**87**:70−106.
27. Li X, Lovell JF, Yoon J, Chen X. Clinical development and potential of photothermal and photodynamic therapies for cancer. *Nat Rev Clin Oncol* 2020;**17**:657−74.
28. Yao C, Wang P, Li X, Hu X, Hou J, Wang L, et al. Near-infrared-triggered azobenzene-liposome/upconversion nanoparticle hybrid vesicles for remotely controlled drug delivery to overcome cancer multidrug resistance. *Adv Mater* 2016;**28**:9341−8.
29. Berg K, Selbo PK, Weyergang A, Dietze A, Prasmickaite L, Bonsted A, et al. Porphyrin-related photosensitizers for cancer imaging and therapeutic applications. *J Microsc* 2005;**218**:133−47.
30. Shen Y, Shuhendler AJ, Ye D, Xu JJ, Chen HY. Two-photon excitation nanoparticles for photodynamic therapy. *Chem Soc Rev* 2016;**45**:6725−41.
31. Torchilin VP. Recent advances with liposomes as pharmaceutical carriers. *Nat Rev Drug Discov* 2005;**4**:145−60.
32. Ma W, Sha SN, Chen PL, Yu M, Chen JJ, Huang CB, et al. A Cell Membrane-targeting self-delivery chimeric peptide for enhanced photodynamic therapy and *in situ* therapeutic feedback. *Adv Healthc Mater* 2020;**9**:1901100.
33. Yu Y, Xu Q, He S, Xiong H, Zhang Q, Xu W, et al. Recent advances in delivery of photosensitive metal-based drugs. *Coord Chem Rev* 2019;**387**:154−79.
34. Shi L, Wang Y, Wang Q, Jiang Z, Ren L, Yan Y, et al. Transforming a toxic drug into an efficacious nanomedicine using a lipoprodrug strategy for the treatment of patient-derived melanoma xenografts. *J Control Release* 2020;**324**:289−302.
35. He M, Yu L, Yang Y, Zou B, Ma W, Yu M, et al. Delivery of triptolide with reduction-sensitive polymer nanoparticles for liver cancer therapy on patient-derived xenografts models. *Chin Chem Lett* 2020;**31**:3178−82.
36. Bruix J, Gores GJ, Mazzaferro V. Hepatocellular carcinoma: clinical frontiers and perspectives. *Gut* 2014;**63**:844−55.
37. Lu J, Wang J, Ling D. Surface engineering of nanoparticles for targeted delivery to hepatocellular carcinoma. *Small* 2018;**14**:1702037.
38. Meng C, Zhu H, Song H, Wang Z, Huang G, Li D, et al. Targets and molecular mechanisms of triptolide in cancer therapy. *Chin J Cancer Res* 2014;**26**:622−6.
39. Luo W, Wen G, Yang L, Tang J, Wang J, Wang J, et al. Dual-targeted and pH-sensitive doxorubicin prodrug-microbubble complex with ultrasound for tumor treatment. *Theranostics* 2017;**7**:452−65.
40. Sheikh Mohamed, Srivani Veeranarayanan, Toru Maekawa, et al. External stimulus responsive inorganic nanomaterials for cancer theranostics. *Adv Drug Deliv Rev* 2019;**138**:18−40.
41. Liu Z, Xie Y, Xiong Y, Liu S, Qiu C, Zhu Z, et al. TLR 7/8 agonist reverses oxaliplatin resistance in colorectal cancer *via* directing the myeloid-derived suppressor cells to tumoricidal M1-macrophages. *Cancer Lett* 2020;**469**:173−85.